JCTC Journal of Chemical Theory and Computation

Distributed Gaussian Valence Bond Surface Derived from Ab Initio Calculations

Jason L. Sonnenberg,[†] Kim F. Wong,[‡] Gregory A. Voth,[‡] and H. Bernhard Schlegel*,[†]

Department of Chemistry, Wayne State University, Detroit, Michigan 48202, and Department of Chemistry, University of Utah, Salt Lake City, Utah 84112

Received November 6, 2008

Ⓦ **This paper contains enhanced objects available on the Internet at http://pubs.acs.org/JCTC.**

Abstract: The experimental and computational results for the tautomerization reaction of 2-pyridone are reviewed. G3, G4, CBS-APNO, and W1 model chemistries are used to generate state-of-the-art reaction energetics for the tautomerization reaction with and without catalytic water molecules in both the gas and aqueous phases. Reactive, electronic potential energy surface surfaces for use in molecular dynamics simulations were generated for these reactions following a recently improved empirical valence bond formulation. The form of molecular mechanics potentials needed for a satisfactory fit is also discussed.

1. Introduction

Over the last century, the keto−enol tautomerism of 2-pyridone (PY) and 2-hydroxypyridine (HY) has been probed by nearly every available experimental[1−13] and theoretical method.[7,10−34] This seemingly innocuous proton-transfer reaction has garnered so much attention because it serves as the archetype model system for hydrogen bonding, proton-transfer tautomerism, and proton-shuttling mechanisms in chemical, biological, and medicinal reactions. Most recently, Hatherley and co-workers used microwave spectroscopy to determine that the gas-phase energy difference between PY and HY is 3.2 ± 0.4 kJ/mol with HY being the more stable species.[8] This value is larger than the ΔG value determined from X-ray photoelectron spectroscopy (PES),[6] but it agrees quite well with Beak's value of 3.3 kJ/mol determined from ultraviolet (UV) spectroscopy.[2] The experimental values are collected in Table 1.

With a gas-phase tautomerization energy smaller than 4.2 kJ/mol (1 kcal/mol, aka chemical accuracy), the PY/HY system has been a formidable challenge for computational chemistry from the beginning. Although semiempirical and molecular mechanics methods provide qualitative agreement with experiment and can describe the PY → HY activation barrier $E^{\ddagger}$ correctly,[15] it was recognized early on that correlation and zero-point vibrational energies are crucial.[16] Following earlier calculations by Schlegel et al. (ref 16), many investigators employed second-order Møller−Plesset perturbation theory (MP2) with a wide variety of basis sets.[10,13,19,21,23,29] While increasing the basis set size beyond triple-ζ (TZ) with the addition of polarization and diffuse functions improved the activation barrier, it unfortunately results in an underestimation of the tautomerization energy because of the well-known correlation energy overestimation by MP2.[35] Predicted tautomerization energies can be brought back into chemical accuracy by utilizing MP4[10] or spin-component-scaled MP2 (SCS-MP2).[36] Density functional theory (DFT) generates reliable molecular structures but the corresponding energetics, with the exception of the BHandHLYP functional,[28,30] are inherently wrong: PY is

Table 1. Experimental Data for the PY → HY Reaction[a]

ΔH	ΔG	T	method	ref
gas phase:				
−3.2 ± 0.4		356	microwave	8
	−3.3	405	UV	2
−2.5 ± 0.4[b]			PES	4
	−2.4 ± 0.21	403	X-ray PES	6
aqueous phase:				
14.2		298	heats of solution	1

[a] Energies and temperatures are in kJ/mol and K, respectively. [b] ΔH was calculated with data ranging from 348 to 728 K using the van't Hoff equation.

* To whom correspondence should be addressed. E-mail: hbs@chem.wayne.edu.

[†] Wayne State University.

[‡] University of Utah.

10.1021/ct800477y CCC: $40.75
Published on Web 03/11/2009

Table 2. Computed Energies (kJ/mol) for the Gas-Phase PY → HY reaction[a]

theory	$\Delta E^{\ddagger}$	$\Delta H^{\ddagger}$	$\Delta G^{\ddagger}$	ΔE	ΔH	ΔG
HF/6-31G(d,p)	207.1[c]			−6.5[h]	−7.3[h]	
HF/6-31++G(d,p)[g]				−5.17	−5.8	
HF/TZV(2df,2dp)[e]				−3.8		
MP2/6-31G(d,p)	147.2[b]	134.0[b]		−9.2[c]		
MP2/6-31+G(d,p)[d]	151.4	138.4	139.4	−8.6	−8.0	
MP2/6-31++G(d,p)[d]	151.3	139.1	144.6	−8.7	−7.1	
MP2/6-311+G(d,p)	149.3	137.3	139.0	−11.6	−10.2	−8.3
MP2/6-311++G(d,p)[d]	149.3			−11.8		
MP2/TZV(2df,2dp)[e]				−11.2		
SCS-MP2/TZV(2df,2dp)//B3LYP/TZV(2df,2dp)[e]				−4.6		
MP4(SDTQ)//MP2/6-311++G(d,p)[f]				−3.62		
CISD/3-21G//HF/3-21G[j]	188.0			12.0		
CISD/DZP1[i]				0.28		
QCISD/TZV(2df,2dp)//B3LYP/TZV(2df,2dp)[e]				−2.9		
QCISD(T)/TZV(2df,2dp)//B3LYP/TZV(2df,2dp)[e]				−4.2		
PBE/TZV(2df,2dp)[e]				6.3		
BP86/TZV(2df,2dp)[e]				5.9		
BLYP/TZV(2df,2dp)[e]				7.9		
B3PW91/6-31++G(d,p)[g]				1.61	1.3	
B3LYP/6-31G(d,p)[b]	148.1	135.0				
B3LYP/6-31+G(d,p)[d]	154.3	140.8	141.3	1.9	1.5	
B3LYP/6-31++G(d,p)[d]	154.2	140.8	141.2	1.8	1.4	
B3LYP/6-311++G(d,p)[d]	158.8	145.1	145.6	3.6	3.3	
B3LYP/6-311++G(2d,2p)[d]	157.6	144.1	144.6	1.5	1.1	1.5
BHandHLYP/6-311++G(2d,2p)[d]	176.6	162.6	163.2	−4.2	−4.6	−4.2
BHandHLYP/TZV(2df,2dp)[e]				−2.9		
G3	159.5	142.3	143.0	−3.8	−4.9	−4.4
G4	156.1	143.1	143.6	−4.2	−4.3	−3.9
CBS-APNO	157.8	144.9	145.1	−4.7	−5.3	−4.9
W1	155.5	142.2	142.7	−3.9	−4.4	−4.1

[a] ΔE is electronic energy and does not include zero-point energy corrections. Enthalpies are at 0 K, while Gibbs free energies are at 298 K. [b] Ref 13. [c] Ref 21. [d] Ref 30. [e] Ref 28. [f] Ref 10. [g] Ref 24. [h] Ref 23. [i] Ref 18. [j] Ref 17.

Table 3. Computed Energies (kJ/mol) for the Gas-Phase $PY(H_2O)_n$ → $HY(H_2O)_n$ Reactions[a]

theory	$\Delta E^{\ddagger}$	$\Delta H^{\ddagger}$	$\Delta G^{\ddagger}$	ΔE	ΔH	ΔG
$PY(H_2O)$ → $HY(H_2O)$:						
HF/6-31G(d,p)[d]	117.2			0.4		
MP2/6-31G(d,p)[b]	57.3			−4.2		
MP2/6-31G(d,p)[d]	55.6			−5.4		
MP2/6-311+G(d,p)	61.3	45.8	51.5	−5.6	−4.4	−3.3
MP2/6-311++G(d,p)[c]				−5.6		
MP4(SDTQ)//MP2/6-311++G(d,p)[c]				1.27		
CISD/3-21G//HF/3-21G[f]	56.0			12.0		
B3LYP/6-31G(d,p)[d]	52.3			3.3		
B3LYP/TZ2P[d]	61.1			5.9		
B3LYP/6-311++G(d,p)[c]				8.65		
B3LYP/6-311++G(2d,2p)[e]	63.1	47.2	52.3	7.1	6.9	7.5
B3LYP/aug-cc-pVTZ//B3LYP/6-311++G(d,p)[c]				7.66		
BHandHLYP/6-311++G(2d,2p)[e]	77.6	60.5	65.9	3.1	2.9	3.5
G3	68.5	51.7	58.0	1.9	0.92	1.4
G4	67.7	52.0	56.1	1.0	0.82	1.2
CBS-APNO	64.0	46.2	52.8	0.98	0.41	0.89
$PY(H_2O)_2$ → $HY(H_2O)_2$:						
MP2/6-31G(d,p)[b]	39.7			−1.3		
MP2/6-311+G(d,p)	69.8	47.2	54.7	1.2	1.9	2.5
CISD/3-21G//HF/3-21G[f]	43.0			19.0		
B3LYP/6-31G(d,p)[d,g]	56.5			13.8		
B3LYP/6-311++G(2d,2p)[e]	67.6	45.4	52.6	12.5	12.1	12.8
BHandHLYP/6-311++G(2d,2p)[e]	85.5	61.4	69.2	9.4	9.0	9.7
G3	75.1	57.3	67.0	4.3	5.7	6.3
G4	77.5	55.0	60.9	7.0	6.2	6.9
$PY(H_2O)_3$ → $HY(H_2O)_3$:						
MP2/6-311+G(d,p)	94.1	67.7	77.3	6.8	6.7	6.5
G3[h]				13.3	12.8	14.7
G4[h]				13.7	14.6	17.5

[a] ΔE is electronic energy and does not include zero-point energy corrections. Enthalpies are at 0 K, while Gibbs free energies are at 298 K. [b] Ref 29. [c] Ref 10. [d] Ref 21. [e] Ref 30. [f] Ref 17. [g] In this calculation, one water is a proton shuttle, and the other is part of the first solvation shell. [h] Transition state calculations were not feasible for this system and level of theory.

predicted to be the most stable tautomer in the gas-phase.[10,13,21,24,28,30,31] Piacenza and Grimme showed convincing evidence that the poor DFT energies arise from the exchange potentials and inclusion of at least 50% Hartree−Fock (HF) exchange "corrects" those exchange potentials as seen in the BHandHLYP results.[28] The necessity of HF exchange in DFT functionals coupled with the MP2 overestimation of the correlation energy suggests that the gas-phase tautomer-

Table 4. Computed Energies (kJ/mol) for the Aqueous Phase $PY(H_2O)_n \rightarrow HY(H_2O)_n$ Reactions[a]

theory	$\Delta E^{\ddagger}$	$\Delta H^{\ddagger}$	$\Delta G^{\ddagger}$	ΔE	ΔH	ΔG
PY → HY:						
MP2/6-311+G(d,p)/IEF-PCM	161.8	148.7	149.6	5.7	5.3	6.0
B3LYP/6-31G(d)/Onsager[c]		158.2[b]	144.8		14.2[b]	13.4
B3LYP/6-311++G(2d,2p)/Onsager[d]			150.1			15.2
B3LYP/6-311++G(2d,2p)/DPCM[d]			176.1			15.4
BHandHLYP/6-311++G(2d,2p)/Onsager[d]			167.7			7.9
BHandHLYP/6-311++G(2d,2p)/DPCM[d]			193.5			10.2
G3/IEF-PCM	168.9	155.0	155.5	14.1	12.4	12.6
G4/IEF-PCM	168.9	155.5	155.9	13.6	12.5	12.7
$PY(H_2O) \rightarrow HY(H_2O)$:						
MP2/6-311+G(d,p)/IEF-PCM	63.9	47.0	53.8	3.1	3.5	4.8
B3LYP/6-31G(d)/Onsager[c]		61.2[b]			11.6[b]	
B3LYP/6-311++G(2d,2p)/Onsager[d]			52.4			13.1
B3LYP6-311++G(2d,2p)/DPCM[d]			70.2			14.6
BHandHLYP/6-311++G(2d,2p)/Onsager[d]			64.7			7.4
BHandHLYP/6-311++G(2d,2p)/DPCM[d]			84.7			13.4
G3/IEF-PCM	73.1	62.2	69.7	12.0	10.8	11.6
G4/IEF-PCM	72.3	55.1	59.6	11.4	10.6	11.0
$PY(H_2O)_2 \rightarrow HY(H_2O)_2$:						
MP2/6-311+G(d,p)/IEF-PCM	71.3	47.7	54.6	4.9	4.9	4.7
B3LYP/6-31G(d)/Onsager[c]		69.5[b]	51.5		17.2[b]	16.4
B3LYP/6-311++G(2d,2p)/Onsager[d]			52.5			15.8
B3LYP/6-311++G(2d,2p)/DPCM[d]			74.6			15.7
BHandHLYP/6-311++G(2d,2p)/Onsager[d]			68.6			12.3
BHandHLYP/6-311++G(2d,2p)/DPCM[d]			94.3			12.9
G3/IEF-PCM	81.7	67.5	77.3	12.2	10.9	11.7
G4/IEF-PCM	80.4	56.1	62.3	11.3	11.2	11.9
$PY(H_2O)_3 \rightarrow HY(H_2O)_3$:						
MP2/6-311+G(d,p)/IEF-PCM	82.4	70.0	78.5	7.6	7.9	8.7
B3LYP/6-31G(d)/Onsager[c]					20.7[b]	19.3
G3/IEF-PCM[e]				13.7	13.2	15.2
G4/IEF-PCM[e]				13.0	11.4	10.9

[a] ΔE is electronic energy and does not include zero-point energy corrections. Enthalpies are at 0 K, while Gibbs free energies are at 298 K unless noted otherwise. [b] Values at 298 K. [c] Ref 31. [d] Ref 30. [e] Transition state calculations were not feasible for this system and level of theory.

ization energetics are dominated by the differences in the exchange energy. Such an illation is supported by HF results that are within chemical accuracy when employing a polarized double-ζ (DZ) or larger basis set.[16,19,21,23,24,28] QCISD, with and without perturbative triples, has predicted tautomerization energies of 4.2 and 2.9 kJ/mol, respectively, indicating that the triples correction is necessary to avoid underestimation of the reaction energy.[28] A representative selection of computational results is presented in Tables 2 and 3.

Because the magnitude of the gas-phase tautomerization barrier prevents rapid proton transfer at room temperature, proton shuttling mechanisms involving explicit water[10,20,21,29−31] and formic acid[13] solvent molecules were investigated. Barone and Adamo were the first to theoretically show that one water molecule reduces the gas-phase tautomerization barrier and switches the lowest energy state from HY to PY.[21] They also demonstrated that addition of a second water molecule to represent bulk solvent actually *increases* the tautomerization barrier because of the hydrogen-bonding interaction with the carbonyl moiety. Maris et al. later confirmed Barone and Adamo's single-molecule proton shuttle findings using MP2, MP4, and DFT methods.[10] One formic acid molecule acting as a proton shuttle was also shown to affect the reaction barrier in the same fashion.[13] In 2005, two groups independently examined the affects of a proton shuttle involving two water molecules and found that both DFT[30] and MP2[29] methods predict a further reduction in the proton-transfer barrier.

Given that inclusion of explicit solvent molecules in addition to those involved in the proton shuttle counterbalances the barrier reduction of the shuttles, a more uniform representation of bulk solvent has been pursued. Wong and co-workers applied the self-consistent reaction field (SCRF) Onsager model to the uncatalyzed 2-pyridone/2-hydroxypyridine tautomerization in cyclohexane and acetonitrile.[19] These results were later confirmed by Wang and Boyd, who also investigated the reaction in chloroform.[22] The same SCRF method was applied to model the tautomerization in water.[21,30,31] For all four solvents, the equilibrium shifts such that the PY species is now favored in solution, which agrees well with experimental results. Barone and Adamo found that inclusion of the bulk solvent via SCRF theory, increased the barrier to proton transfer and stabilized PY for the single water molecule shuttle with and without an explicit solvation shell water.[21] Fu et al. also observed such effects for one and two water proton shuttles.[30] Tsuchida and Yamabe[31] continued the energetic exploration of multiwater proton shuttles in solution and reported that a three-molecule proton shuttle actually *increases* the tautomerization barrier relative to the two-molecule shuttle rather than reducing it. Unfortunately the reported three-molecule proton shuttle transition state (TS) corresponds to a proton transfer between the three

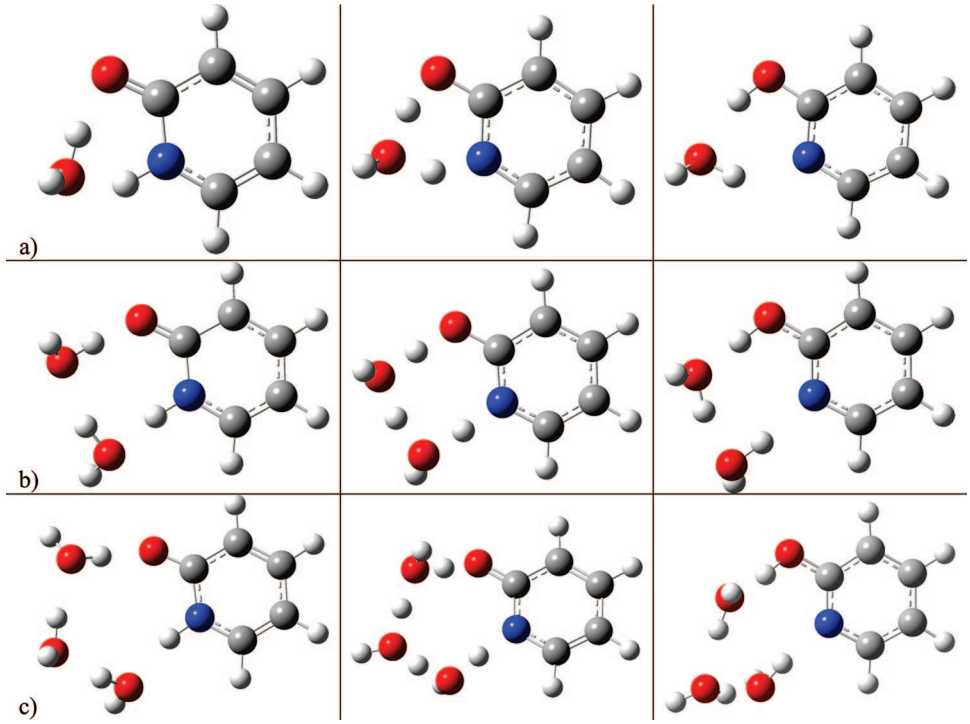

Figure 1. PY$(H_2O)_n$ (reactant), TS$(H_2O)_n$ (transition state), and HY$(H_2O)_n$ (product) geometries for proton-shuttling tautomerization reactions with (a) one, (b) two, and (c) three catalytic water molecules. Carbon, nitrogen, oxygen, and hydrogen are depicted in gray, blue, red, and white, respectively.

Ⓦ Movies of the molecules shown in panels a, b, and c along the reaction paths are available.

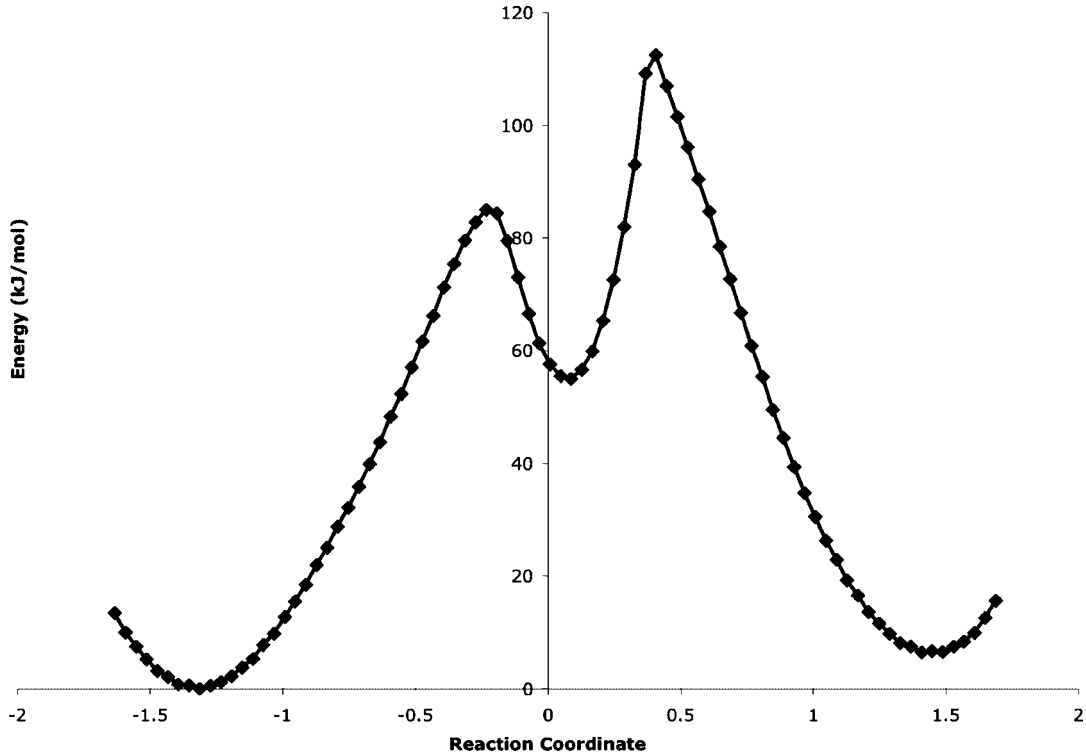

Figure 2. Potential of mean force along the reaction path for the gas-phase, uncatalyzed PY → HY tautomerization employing the $K = 5$ DG-EVB surface. The artificial minimum near the TS results from the quadratic forms of H_{11} and H_{22}.

water molecules rather than true proton shuttling. The correct TS for the three-water proton shuttle for the PY to HY tautomerization is included in Tables 3 and 4 and the structure is available in the Supporting Information for the present paper.

This paper provides benchmark reaction energetics for the PY$(H_2O)_n$ → HY$(H_2O)_n$ ($n = 0-3$) tautomerization reactions in the gas and solution phases. The influence of proton-shuttling water molecules in both phases is also discussed. A reactive electronic potential energy surface for use in

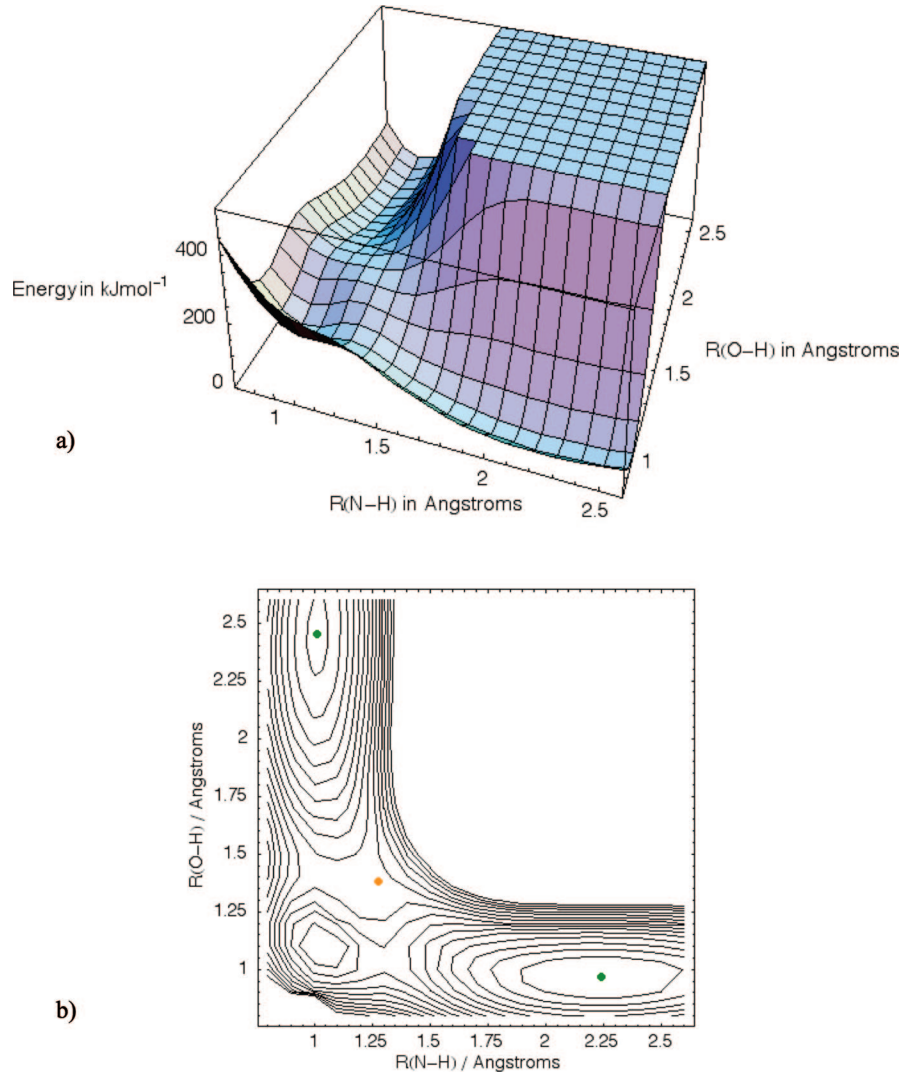

Figure 3. Two-dimensional DG-EVB potential energy surface for the gas-phase, uncatalyzed PY → HY tautomerization, employing the $K = 5$ fit with quadratic H_{nn}. The PY valley is in the back, left-hand corner, while the HY valley is up front in the right-hand corner in both plots. The minima are denoted with a green dot and the TS with an orange dot.

molecular dynamics simulations is then generated from the highly accurate ab initio results following a recently improved EVB formulation using a superposition of states[37,38] and distributed Gaussians.[39,40] The importance of utilizing improved molecular mechanics force fields that go beyond the quadratic approximation utilized in most dynamics calculations is addressed.

2. Computational Methods

The G3,[41] G4,[42] CBS-APNO,[43] and W1[44] model chemistries were employed to determine tautomerization energetics to within ±4.7, ±3.5, ±2.2, and ±1.3 kJ/mol, respectively. Additional data points along the reaction path were generated at the MP2/6-311+G(d,p) level of theory[45−47] using the second-order predictor-corrector reaction path following integrator of Hratchian and Schlegel.[48,49] All stationary points along the reaction path were optimized with the Berny algorithm[50] and confirmed with harmonic vibrational frequency analysis. Bulk solvation effects were accounted for via IEF-PCM in the SCRF framework with a dielectric value of 78.39 and UFF atomic radii.[51−53] All electronic structure calculations were computed using a development version of the Gaussian suite,[54] while the EVB fits and analysis were done in Mathematica version 5.2[55] using the EVB Toolkit for Mathematica[56] developed by the authors. Preliminary MD calculations employed the development version of AMBER 10.[57]

3. Results and Discussion

The discussion begins with calculated results for the pyridone tautomerization reaction, in both the gas and aqueous phases, which has been studied extensively. The effect of proton shuttling waters on reaction energetics and barrier heights is examined for one to three catalytic waters. A new TS structure for the proton-shuttling mechanism involving three catalytic water molecules is given to correct an existing error in the literature. The general form of valence bond potential surfaces for reactions is described, and then some technical aspects of building reliable reactive potential energy surfaces are discussed.

3.1. Reaction Energetics. Our gas- and aqueous-phase results for the pyridone tautomerization are presented in

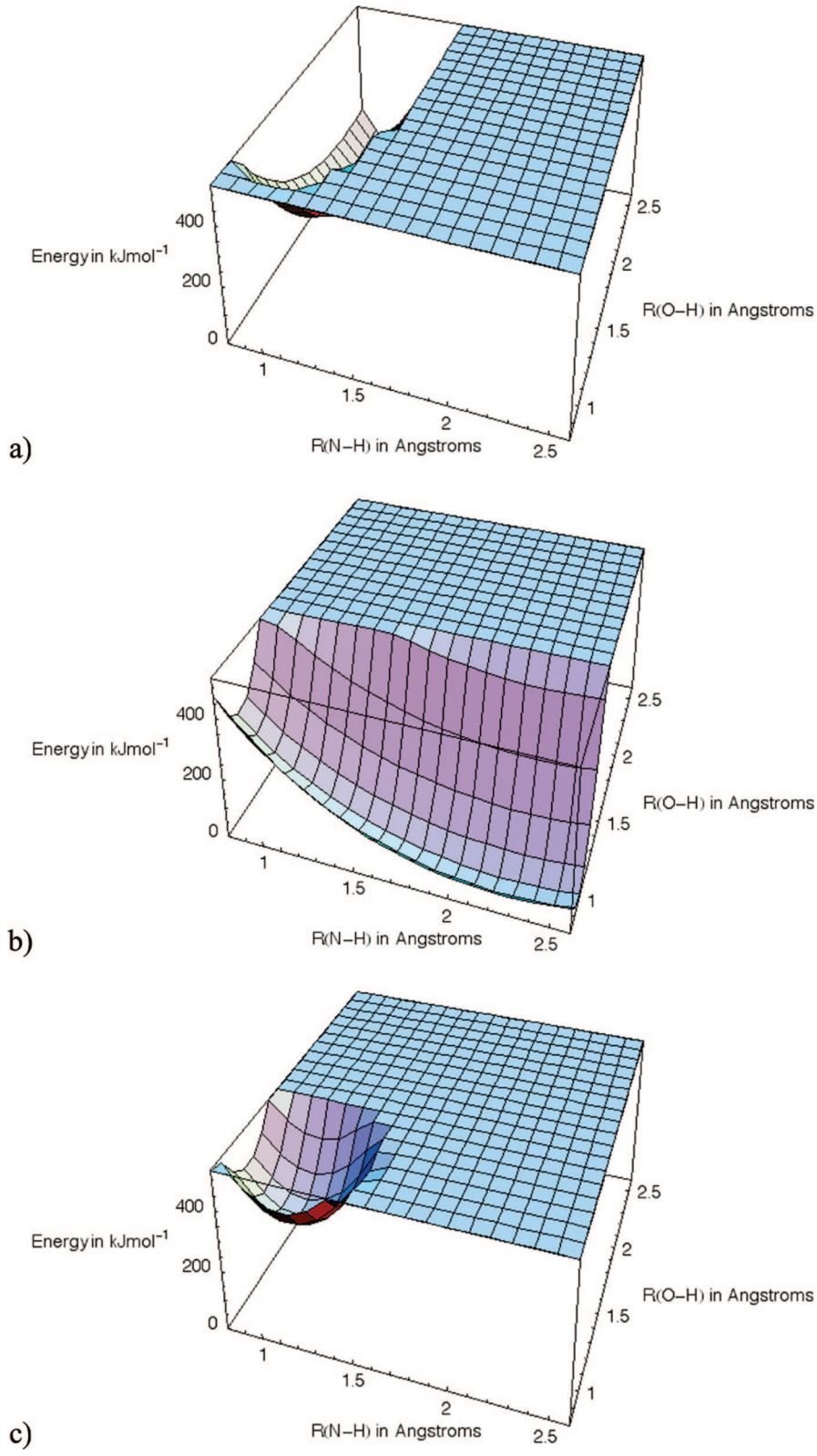

Figure 4. Decomposition of the DG-EVB potential energy surface for the gas-phase, uncatalyzed PY → HY tautomerization employing the $K = 5$ fit with quadratic H_{nn}: (a) H_{11}, (b) H_{22}, and (c) the first term of eq 4, $(H_{11} + H_{22})/2$. The PY valley is in the back, left-hand corner, while the HY valley is up front in the right-hand corner in all plots.

Tables 2−4. For the uncatalyzed tautomerization, the system size is small enough that all four model chemistries, G3, G4, CBS-APNO, and W1 are tractable calculations. Differences of less than 1 kJ/mol between theory and experiment should be considered excellent agreement for systems of this size, thus the gas-phase W1 results can be taken as a "gold standard" for evaluation of other computed results. Of the three remaining model chemistries, the error in barrier heights and reaction energetics increases as G4 < G3 < CBS-APNO when compared to the W1 results. Although CBS-APNO calculations were still feasible for the gas-phase tautomerization reaction catalyzed with one water molecule, only G3

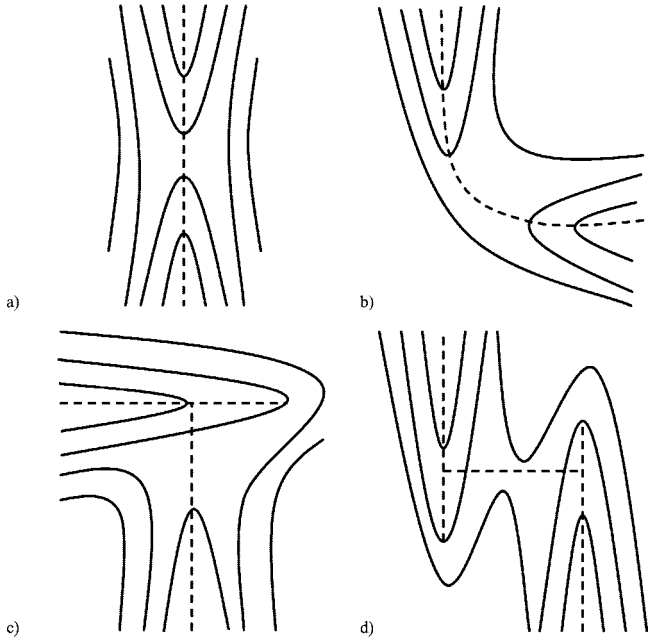

Figure 5. Various classes of reaction channels near the TS on reactive potential energy surfaces: (a) I-shaped valley, (b) L- or V-shaped valley, (c) T-shaped valley, (d) H- or X-shaped valley.

and G4 model chemistry results were computed for gas-phase reactions with more than one water molecule and for all aqueous reactions. For the aqueous results, the agreement between G4 and experiment is very good for the uncatalyzed tautomerization, thus all further discussions of energetics will refer to the G4 results unless noted otherwise.

As seen previously,[10,21] HY is the lower energy gas-phase tautomer only when no proton-shuttling water is present. The addition of one, two, or three water catalysts stabilizes PY by an additional 5.2, 6.0, and 6.7 kJ/mol, respectively. Interestingly, the catalytic waters always form a prereactive complex which minimizes the hydrogen bonding distances prior to transferring the H atom (see Supporting Information). In the aqueous systems, PY is always the lower energy tautomer regardless of the number of catalytic water molecules present. As seen in Table 4, the aqueous reaction energy computed with polarizable continuum models becomes essentially constant once catalytic water molecules are employed as proton shuttles. Therefore the number of catalytic water molecules actually participating in the ground-state tautomerization reaction is determined by the barrier height, *not* the over all reaction energy. Such trends in reaction barriers for additional catalytic waters have been seen previously.[58] In both phases, the reaction barrier decreases by ~90 kJ/mol with the addition of one catalytic water molecule. Additional water molecules actually *increase* the barrier height by ~10 kJ/mol for two water molecules, which agrees with earlier computational studies.[21,30] Since multiple water catalysts increase the reaction barrier height, electronic potential energy surfaces will only be constructed for the two reactions, PY → HY and PY(H_2O) → HY(H_2O).

3.2. Reactive Potential Energy Surfaces. A prerequisite step in molecular dynamic (MD) studies is the construction of a reliable reactive electronic potential energy surface. A reactive potential energy surface $V(\mathbf{q})$, where $\mathbf{q}$ is the vector of molecular coordinates, can be constructed by means of a superposition of reactant and product configuration, ψ_1 and ψ_2, interacting via an empirical Hamiltonian, $\hat{\mathbf{H}}$.[59]

$$\Psi = c_1\psi_1 + c_2\psi_2 \tag{1}$$

$$\hat{\boldsymbol{H}} = \begin{bmatrix} H_{11} & H_{12} \\ H_{21} & H_{22} \end{bmatrix} \tag{2}$$

$$H_{11} = \langle\psi_1|\hat{H}|\psi_1\rangle, H_{12} = H_{21} = \langle\psi_1|\hat{H}|\psi_2\rangle, H_{22} = \langle\psi_2|\hat{H}|\psi_2\rangle \tag{3}$$

$$V(\mathbf{q}) = \tfrac{1}{2}[H_{11}(\mathbf{q}) + H_{22}(\mathbf{q})] - \sqrt{\{\tfrac{1}{2}[H_{11}(\mathbf{q}) - H_{22}(\mathbf{q})]\}^2 + H_{12}^2(\mathbf{q})} \tag{4}$$

H_{11} and H_{22} are the energy surfaces for the reactant and product potentials, respectively, and H_{12} is the resonance integral that must be represented by an approximate functional form. The construction of reactive potential energy surfaces as a superposition of two or more states has a long history as evidenced in the review by Balint-Kurti.[60] In 1929, London showed that a qualitatively correct potential energy surface for the H + H_2 exchange reaction could be generated from two configurations.[61] In a 1938 Faraday discussion on reaction kinetics, Eyring reported the potential energy surface for the same hydrogen exchange reaction calculated from the interaction of five configurations.[62] At the same conference, Evans and Polanyi described a surface for the Cl^- + CH_3Cl S_N2 reaction built from a reactant and a product configuration.[63] The ensuing discussion pointed out that the two approaches are equivalent and identical to the method used in an earlier work on the barriers for ionic reactions.[64] Evans also provided an early application of this approach to the Diels−Alder reaction.[65] Subsequent variations on this method differ primarily in the manner of approximating the H_{11}, H_{22}, and H_{12} matrix elements.

An empirical valence bond (EVB) approach for estimating the matrix elements was employed by Warshel for comparing reactions in solution and enzymes.[66] Pross and Shaik used a qualitative, valence-bond, configuration-mixing approach to investigate organic reactions.[67] More relevant to the present work, Chang and Miller[68,69] constructed accurate potential energy surfaces by fitting a superposition of two EVB configurations to ab initio energies, gradients and Hessians using a generalized Gaussian for H_{12}. Minichino and Voth generalized the Chang-Miller method[68] for N-state systems and provided a scheme to correct gas-phase ab initio data for solutions.[70]

From a pedagogical point of view, EVB surfaces can be classified by the approximation employed in H_{12}. In addition to the simple choice of setting H_{12} equal to a constant (Constant-EVB) that reproduces experimental or high-level ab initio barrier heights, two methods have emerged for constructing accurate reactive EVB surfaces: DWI-EVB and DG-EVB. DWI-EVB represents $H_{12}(\mathbf{q})$ as a distance weighted interpolation (DWI), aka Shepard interpolation, around a set of molecular configurations (called Shepard points) where the energy, gradient, and Hessian are available.[71−74] DG-EVB builds upon the Chang−Miller method[68] and expands

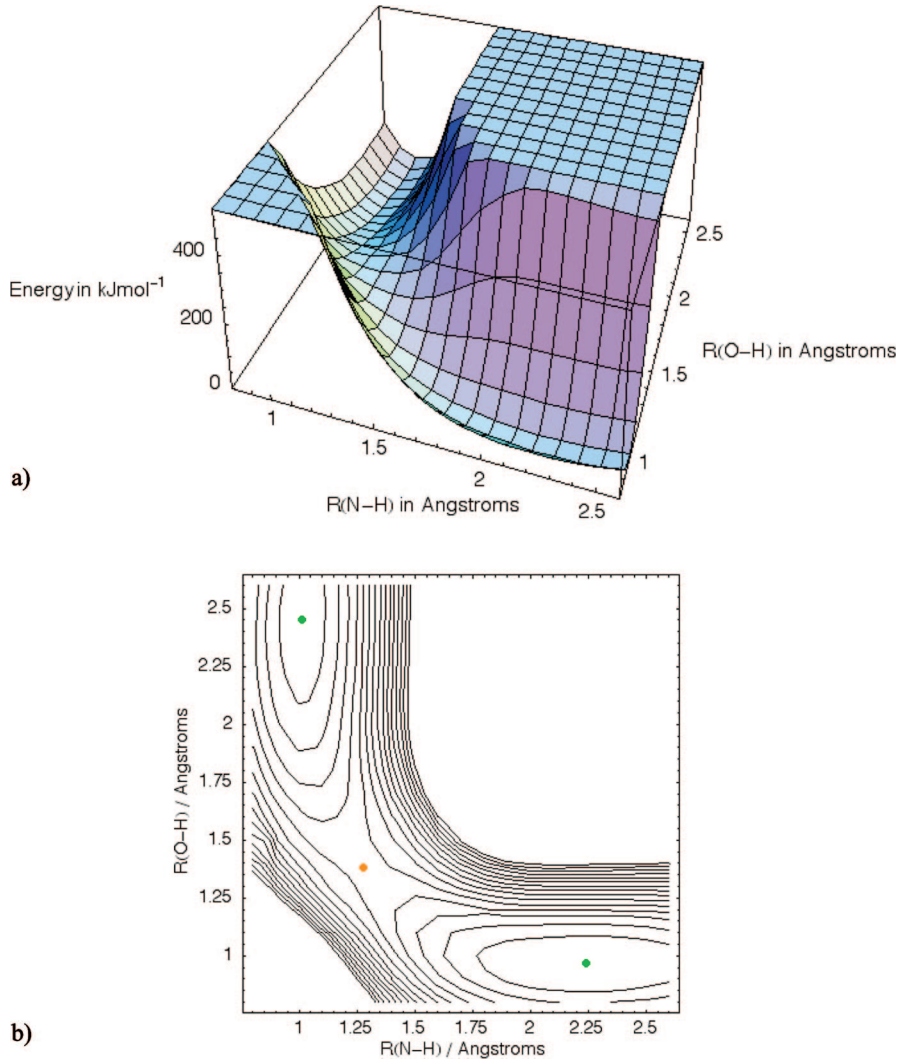

Figure 6. Two-dimensional DG-EVB potential energy surface for the gas-phase, uncatalyzed PY → HY tautomerization employing the $K = 5$ fit with repulsive H_{nn}. The PY valley is in the back, left-hand corner, while the HY valley is up front in the right-hand corner in both plots. The minima are denoted with a green dot and the TS with an orange dot.

$H^2_{12}(\mathbf{q})$ into a set of distributed Gaussians (DG) centered on a set of molecular configurations.[39,40] In our DG-EVB approach, the following form of $H^2_{12}(\mathbf{q})$ is used to reproduce electronic structure data,

$$H^2_{12}(\mathbf{q}) = \sum_{K}^{N_{\mathrm{cfg}}} \sum_{i \geq j \geq 0}^{N_{\mathrm{dim}}} B_{ijK} g(\mathbf{q}, \mathbf{q}_K, i, j, \alpha_K) \tag{5}$$

$$H^2_{12}(\mathbf{q}) = [H_{11}(\mathbf{q}) - V(\mathbf{q})][H_{22}(\mathbf{q}) - V(\mathbf{q})] \tag{6}$$

$$\Delta\mathbf{q}_K = \mathbf{q} - \mathbf{q}_K \tag{7}$$

$$\begin{aligned} g(\mathbf{q}, \mathbf{q}_K, 0, 0, \alpha_K) &= (1 + \tfrac{1}{2}\alpha_K|\Delta\mathbf{q}_K|^2)\exp[-\tfrac{1}{2}\alpha_K|\Delta\mathbf{q}_K|^2] \\ g(\mathbf{q}, \mathbf{q}_K, i, 0, \alpha_K) &= (\Delta\mathbf{q}_K)_i \exp[-\tfrac{1}{2}\alpha_K|\Delta\mathbf{q}_K|^2] \\ g(\mathbf{q}, \mathbf{q}_K, i, j, \alpha_K) &= (1 - \tfrac{1}{2}\delta_{ij})(\Delta\mathbf{q}_K)_i(\Delta\mathbf{q}_K)_j \exp[-\tfrac{1}{2}\alpha_K|\Delta\mathbf{q}_K|^2] \end{aligned} \tag{8}$$

where $g(\mathbf{q}, \mathbf{q}_K, i, j, \alpha_K)$ are s-, p-, and d-type Gaussians centered at a number of molecular configurations, $\mathbf{q}_K$, on the potential energy surface and $\mathbf{B}$ is a vector of coefficients. It is important to note that nonstandard s- and d-type Gaussians are employed to precondition the resulting set of linear equations (see Appendix) that are passed to a GMRES[75] (aka DIIS[76−78]) solver. For a more exhaustive discussion of the DG-EVB method please see ref 39.

Previously the gas-phase, uncatalyzed, 2-pyridone tautomerization reaction was utilized as a test system for the DG-EVB method employing a GMRES solver.[40] In that work, a simple quadratic function was employed for H_{11} and H_{22}

$$H_{nn}(\mathbf{q}) = E_n + \mathbf{g}_n^{\mathrm{T}}\cdot\Delta\mathbf{q} + \tfrac{1}{2}(\Delta\mathbf{q}^{\mathrm{T}}\cdot\tilde{\mathbf{H}}_n\cdot\Delta\mathbf{q}), \quad \Delta\mathbf{q} = \mathbf{q} - \mathbf{q}_n \tag{9}$$

where E_n, $\mathbf{g}_n$, and $\tilde{\mathbf{H}}_n$ are the ab initio energy, gradient, and Hessian, respectively, of the reactant or product. Preliminary MD calculations using the published distributed-Gaussian surfaces discovered a false minimum in the potential of mean force (PMF) plot shown in Figure 2, as a result of an oversimplified form for H_{11} and H_{22}. To investigate the artificial minimum in the PMF plot, a two-dimensional relaxed scan of the 2-pyridone N−H and O−H bond lengths was computed at the HF/6−311+G(d,p) level of theory. The resulting DG-EVB surface for those HF geometries indicated

that a "swimming hole" had formed behind the TS (see Figure 3). The source of the "swimming hole", as shown in Figure 4, was the interaction of H_{11} and H_{22} in the first term of eq 4. Although H_{12} can correct H_{11} and H_{22}, thereby producing an improved V along the reaction path, it cannot completely counterbalance the additive interaction of the quadratic valence bond potentials near the TS. For L- or V-shaped reaction channels, arising from reactions where two coordinates dominate the reaction path, as in the pyridone tautomerization, a simple quadratic potential is too rudimentary and could generate artificial holes in the EVB surface. The T-, H-, or X-shaped reaction channels[80] shown in Figure 5 may also generate artificial minima in the DG-EVB surface when simple quadratic potentials are used as a consequence of geometry, but I-shaped reaction channels should not.

The ground-state potential generated by the interaction of H_{11} and H_{22} via H_{12} is given in eq 4. For this expression to be a good model of the true potential, $V_{\text{true}}(\mathbf{q})$, the first term must always be greater than $V_{\text{true}}(\mathbf{q})$, since the square root in the second term must be positive and real for the ground-state potential.

$$\tfrac{1}{2}(H_{11}(\mathbf{q}) + H_{22}(\mathbf{q})) \geq V_{\text{true}}(\mathbf{q}) \tag{10}$$

In the region around the TS or around any test point, we can approximate $V_{\text{true}}(\mathbf{q})$ by a Taylor series truncated at second order

$$V_{\text{TS}}(\mathbf{q}) \approx V_{\text{TS}}^0 + (\mathbf{V}_{\text{TS}}')^{\text{T}}(\mathbf{q} - \mathbf{q}_{\text{TS}}) + \tfrac{1}{2}(\mathbf{q} - \mathbf{q}_{\text{TS}})^{\text{T}}\tilde{\mathbf{V}}_{\text{TS}}''(\mathbf{q} - \mathbf{q}_{\text{TS}}) \tag{11}$$

with trust radius $\boldsymbol{\tau}_{\text{TS}}$ defining the region where the approximation is valid. The sum of $H_{11}(\mathbf{q})$ and $H_{22}(\mathbf{q})$ can also be approximated by a quadratic function around the TS.

$$V_{\text{sum}}(\mathbf{q}) = \frac{H_{11}(\mathbf{q}) + H_{22}(\mathbf{q})}{2} \approx V_{\text{sum}}^0 + (\mathbf{V}_{\text{sum}}')^{\text{T}}(\mathbf{q} - \mathbf{q}_{\text{TS}}) + \tfrac{1}{2}(\mathbf{q} - \mathbf{q}_{\text{TS}})^{\text{T}}\tilde{\mathbf{V}}_{\text{sum}}''(\mathbf{q} - \mathbf{q}_{\text{TS}}) \tag{12}$$

Note that the minimum for $V_{\text{sum}}(\mathbf{q})$ is between the minima for $H_{11}(\mathbf{q})$ and $H_{22}(\mathbf{q})$, that is, possibly but not necessarily near the transition state. The quadratic expansions for $V_{\text{sum}}(\mathbf{q})$ and $V_{\text{TS}}(\mathbf{q})$ can now be compared to see if eq 4 can produce a suitable surface with the given potentials for $H_{11}(\mathbf{q})$ and $H_{22}(\mathbf{q})$. In particular, we require $V_{\text{sum}}(\mathbf{q}) - V_{\text{TS}}(\mathbf{q}) \geq 0$ to satisfy equation 10.

$$\begin{aligned}
&V_{\text{sum}}(\mathbf{q}) - V_{\text{TS}}(\mathbf{q}) = V_{\text{diff}}(\mathbf{q}) = \\
&V_{\text{diff}}^0 + (\mathbf{V}_{\text{diff}}')^{\text{T}}(\mathbf{q} - \mathbf{q}_{\text{TS}}) + \tfrac{1}{2}(\mathbf{q} - \mathbf{q}_{\text{TS}})^{\text{T}}\tilde{\mathbf{V}}_{\text{diff}}''(\mathbf{q} - \mathbf{q}_{\text{TS}}) \\
&V_{\text{diff}}^0 = (V_{\text{sum}}^0 - V_{\text{TS}}^0), \\
&\mathbf{V}_{\text{diff}}' = (\mathbf{V}_{\text{sum}}' - \mathbf{V}_{\text{TS}}'), \tilde{\mathbf{V}}_{\text{diff}}'' = (\tilde{\mathbf{V}}_{\text{sum}}'' - \tilde{\mathbf{V}}_{\text{TS}}'') \\
&\mathbf{q}_{\text{min}} = -(\tilde{\mathbf{V}}_{\text{diff}}'')^{-1}\mathbf{V}_{\text{diff}}', \\
&V_{\text{diff}}(\mathbf{q}_{\text{min}}) = V_{\text{diff}}^0 - \tfrac{1}{2}\mathbf{V}_{\text{diff}}'(\tilde{\mathbf{V}}_{\text{diff}}'')^{-1}\mathbf{V}_{\text{diff}}'
\end{aligned} \tag{13}$$

where $\mathbf{q}_{\text{min}}$ is the minimum of $V_{\text{diff}}(\mathbf{q})$ (or a higher order stationary point if $\tilde{V}_{\text{diff}}''$ has one or more negative eigenvalues). A number of cases can be considered.

(a) If $V_{\text{diff}}(\mathbf{q}_{\text{min}})$ is positive and all the eigenvalues of $\tilde{\mathbf{V}}_{\text{diff}}''$ are positive, then eq 10 holds for all $\mathbf{q}$ within the trust region of the quadratic expansion and a reliable potential energy surface can be constructed in this region with a suitable choice for $H_{12}^2(\mathbf{q})$ (however, this may require additional molecular configurations).

(b) If $V_{\text{diff}}(\mathbf{q}_{\text{min}})$ is negative or some of the eigenvalues of $\tilde{\mathbf{V}}_{\text{diff}}''$ are negative, then eq 10 is not satisfied in some regions. This can lead to a "swimming hole" similar to the one observed in the simple potential for pyridone. This can be analyzed further by determining where $V_{\text{diff}}(\mathbf{q})$ is negative.

(i) If $V_{\text{diff}}(\mathbf{q}_{\text{min}})$ is negative and $\mathbf{q}_{\text{min}}$ is within the trust radius of the transition state, $|\mathbf{q}_{\text{min}} - \mathbf{q}_{\text{TS}}| < \boldsymbol{\tau}_{\text{TS}}$, then there is clearly a problem.

(ii) For other cases, one needs to find the minimum of $V_{\text{diff}}(\mathbf{q})$ with the constraint $|\mathbf{q}_{\text{min}} - \mathbf{q}_{\text{TS}}| = \boldsymbol{\tau}_{\text{TS}}$. If $V_{\text{diff}}(\mathbf{q}_{\text{min}}) < 0$ for this constrained minimization, then there is a problem. Even if $V_{\text{diff}}(\mathbf{q}_{\text{min}}) > 0$, there may still be problems outside the trust region of the transition state, especially if some of the eigenvalues of $\tilde{\mathbf{V}}_{\text{diff}}''$ are negative. In this case, the location of $\mathbf{q}_{\text{min}}$ may suggest regions for additional molecular configurations to test the surface and to fit $H_{12}^2(\mathbf{q})$.

The analysis described above can be repeated for any additional points used for fitting the surface. It should be emphasized that if eq 10 is not satisfied, the form of $H_{11}(\mathbf{q})$ and $H_{22}(\mathbf{q})$ *must* be modified to avoid spurious deformations of the surface. This is *independent* of the model used for $H_{12}(\mathbf{q})$ and the resulting EVB surface (e.g., DWI-EVB and DG-EVB).

To improve our model valence bond potentials and bring them more in line with modern molecular mechanics potentials, a nonbonding, van der Waals, exponential-6 term from the universal force field (UFF)[80] was added to H_{nn} for coordinates of interest.

$$\begin{aligned}
&H_{nn}(\mathbf{q}) = \\
&C + \mathbf{g}_n^{\text{T}}\cdot\Delta\mathbf{q} + \tfrac{1}{2}(\Delta\mathbf{q}^{\text{T}}\cdot\tilde{\mathbf{H}}_n\cdot\Delta\mathbf{q}) + \sum_i A_{\text{UFF}}^i \exp[-B_{\text{UFF}}^i\Delta\mathbf{q}^i] \\
&\Delta\mathbf{q} = \mathbf{q} - \mathbf{q}_n, C = E_n - \sum_i A_{\text{UFF}}^i \exp[-B_{\text{UFF}}^i\Delta\mathbf{q}^i]
\end{aligned} \tag{14}$$

In eq 14, A_{UFF}^i and B_{UFF}^i are UFF exponential-6 parameters, $\Delta\mathbf{q}^i$ is the repulsive coordinate value (e.g., H—O in PY and N—H in HY) for H_{nn}, and C is a constant ensuring the ab initio energy is recovered at the DG-EVB data points, $\mathbf{q} = \mathbf{q}_n$. Alternatively, the harmonic bond-stretch terms could be replaced by Morse potentials but this requires the determination of Morse parameters for bonds of interest. Both capabilities have been added to the development version of AMBER 10, so that eq 10 can be satisfied. The exponential-6 term has the advantage of less work because all the necessary parameters are already in the literature. In Figure 6, it can been seen that the additional repulsive term does remove the "swimming hole" behind the TS. Since the α values for the $K = 5$ DG-EVB fit are nearly independent of the form of H_{nn}, simple quadratic valence bond potentials may be useful in accelerating the α values optimization process for very large molecular systems, such as enzymes.

The improved form of H_{nn} was utilized to build a DG-EVB surface for the pyridone tautomerization catalyzed by a proton-shuttling water in the gas phase. With $K = 5$, α values of {1.2, 1.3, 1.9, 1.8, 1.8} and four repulsive coordinates, the maximum error along the reaction path is 2.37 kJ/mol. The absence of artificial "swimming holes" in the surface indicates that our improved H_{nn} is acceptable for the current application. It is important to note that one should always test the accuracy both on and off of the reaction path to ensure the quality of the surface.

4. Conclusions

This work reviewed the experimental and computational results for the tautomerization reaction of 2-pyridone. State of the art G3, G4, CBS-APNO, and W1 model chemistries were employed along with the IEF-PCM method to elucidate the gas- and solution-phase tautomerization reaction energetics with and without proton shuttling water molecules. The new data clearly show how the addition of both catalytic water and bulk solvent renders the tautomerization energy in solution nearly constant at 11 kJ/mol in favor of $PY(H_2O)_n$. Since the reaction energy is nearly constant, the reaction barrier correlates with the number of catalytic water molecules employed in the tautomerization. Again it is clear that while reaction channels employing two and three proton-shuttling waters are possible, these channels actually have *higher* barriers than the reaction path utilizing one catalytic water.

Reactive electronic potential energy surfaces suitable for use in molecular dynamics simulations were generated for PY → HY and $PY(H_2O)$ → $HY(H_2O)$ reactions using the DG-EVB formalism. Investigation of our previously published PY → HY surface illuminated a shortcoming in our ground-state molecular mechanics potentials, namely that harmonic force fields do not guarantee an EVB surface free of spurious deformations. This shortcoming can be overcome by including a repulsive term in the force field for at least the bonds that are breaking and forming. This new form of H_{nn} was successfully used to generate new DG-EVB surfaces that possess no artificial minima along or besides the reaction path. Employing a H_{nn} functional form that satisfies eq 10 lays the foundation for applying the DG-EVB methodology to large-scale biological simulations.

Acknowledgment. The Office of Naval Research (N00014-05-1-0457) supported this research. The authors thank Dr. Shinichi Yamabe for providing his three-water proton shuttle TS and are grateful for computer time from the Wayne State University Grid.

Supporting Information Available: The EVB Toolkit for Mathematica is free software available for download along with all DG-EVB surfaces on the "Software" tab at http://chem.wayne.edu/schlegel/. Cartesian coordinates of the stationary points along with animated GIFs of the gas-phase, MP2 IRC geometries for the four, tautomerization reactions. This material is available free of charge via the Internet at http://pubs.acs.org.

Appendix

For a symmetric 2 × 2 EVB Hamiltonian matrix,

$$\hat{\mathbf{H}}_{\mathrm{EVB}} = \begin{bmatrix} H_{11} & H_{12} \\ H_{21} & H_{22} \end{bmatrix} \tag{15}$$

the analytical solution for the coupling term is

$$H_{12}^2(\mathbf{q}) = [H_{11}(\mathbf{q}) - \varepsilon_{\mathrm{EVB}}(\mathbf{q})][H_{22}(\mathbf{q}) - \varepsilon_{\mathrm{EVB}}(\mathbf{q})] \tag{16}$$

where $\varepsilon_{\mathrm{EVB}}$is the lowest eigenvalue of the matrix and $H_{11}(\mathbf{q})$ and $H_{22}(\mathbf{q})$ are the reactant and product valence bond states. $H_{11}(\mathbf{q})$ and $H_{22}(\mathbf{q})$ can be described by a force field potential or as a Taylor series expansion about the minimum from ab initio calculations. With the valence bond states defined, the goal here is to provide a prescription for $H_{12}^2(\mathbf{q})$ such that the resulting EVB surface approximates the ab initio surface, that is, $\varepsilon_{\mathrm{EVB}} = \varepsilon_{\Psi}$. The Chang−Miller approach approximates $H_{12}^2(\mathbf{q})$ as a generalized Gaussian

$$H_{12}^2(\mathbf{q}) = A \exp[\mathbf{B}^{\mathrm{T}}\cdot\Delta\mathbf{q} - \tfrac{1}{2}\Delta\mathbf{q}^{\mathrm{T}}\cdot\tilde{\mathbf{C}}\cdot\Delta\mathbf{q}], \Delta\mathbf{q} = \mathbf{q} - \mathbf{q}_{\mathrm{TS}} \tag{17}$$

where the parameters A (a scalar), $\mathbf{B}$ (a vector), and $\tilde{\mathbf{C}}$ (a matrix) are chosen to reproduce the ab initio energy, gradient, and Hessian at the transition state. In this form, H_{12}^2 diverges for large $\Delta\mathbf{q}$ when $\tilde{\mathbf{C}}$ contains one or more negative eigenvalues. While refinements are available for controlling the asymptotic behavior of the Chang−Miller approach, recasting eq 17 in terms of a quadratic polynomial times a spherical Gaussian

$$H_{12}^2(\mathbf{q}) = A[1 + \mathbf{B}^{\mathrm{T}}\cdot\Delta\mathbf{q} + \tfrac{1}{2}\Delta\mathbf{q}^{\mathrm{T}}\cdot(\tilde{\mathbf{C}} + \alpha\tilde{\mathbf{I}})\cdot\Delta\mathbf{q}]\exp[-\tfrac{1}{2}\alpha|\Delta\mathbf{q}|^2] \tag{18}$$

keeps the coupling element bounded at the asymptotes. The distributed Gaussian (DG) approach generalizes the above polynomial times a Gaussian prescription to utilize ab initio information at other potential energy surface points in addition to the transition state. Here, $H_{12}^2(\mathbf{q})$ is approximated as an expansion about a set of distributed Gaussians centered on a set of molecular configurations $\mathbf{q}_K$

$$H_{12}^2(\mathbf{q}) = \sum_{K}^{N_{\mathrm{cfg}}} \sum_{i\geq j\geq 0}^{N_{\mathrm{dim}}} B_{ijK} g(\mathbf{q}, \mathbf{q}_K, i, j, \alpha_K) \tag{19}$$

$$g(\mathbf{q}, \mathbf{q}_K, 0, 0, \alpha_K) = (1 + \tfrac{1}{2}\alpha_K|\Delta\mathbf{q}_K|^2)\exp[-\tfrac{1}{2}\alpha_K|\Delta\mathbf{q}_K|^2] \tag{20}$$

$$g(\mathbf{q}, \mathbf{q}_K, i, 0, \alpha_K) = (\Delta\mathbf{q}_K)_i \exp[-\tfrac{1}{2}\alpha_K|\Delta\mathbf{q}_K|^2] \tag{21}$$

$$g(\mathbf{q}, \mathbf{q}_K, i, j, \alpha_K) = (1 - \tfrac{1}{2}\delta_{ij})(\Delta\mathbf{q}_K)_i(\Delta\mathbf{q}_K)_j \exp[-\tfrac{1}{2}\alpha_K|\Delta\mathbf{q}_K|^2] \tag{22}$$

$$\Delta\mathbf{q}_K = \mathbf{q} - \mathbf{q}_K \tag{23}$$

where N_{cfg} is the number of ab initio data points used for the fitting, N_{dim} is the number of system coordinates, $g(\mathbf{q},\mathbf{q}_K,i,j,\alpha_K)$ are the s-, p-, and d-type Gaussians and B_{ijK} are the expansion coefficients. The term involving the unit matrix in eq 18 was accumulated into the s-type Gaussian

(eq 20) to precondition the system of linear equations for faster convergence when utilizing iterative solution methods. The non-standard form of the d-type Gaussian is for similar reasons. If the number of Gaussian centers K is equal to the number of data points where H_{12}^2 are evaluated, eq 19 describes a system of linear equations

$$\mathbf{F}^{\mathrm{T}} = \mathbf{B}^{\mathrm{T}}\tilde{\mathbf{D}}^{\mathrm{T}}$$

or

$$\mathbf{F} = \tilde{\mathbf{D}}\mathbf{B} \quad (24)$$

that can be solved using singular value decomposition or by an iterative procedure, such as GMRES. The vector $\mathbf{F}$ stores the coupling terms evaluated at the N_{cfg} ab initio configurations

$$\mathbf{F} = \begin{bmatrix} H_{12}^2(\mathbf{q}_1) \\ H_{12}^2(\mathbf{q}_2) \\ \vdots \\ H_{12}^2(\mathbf{q}_{N_{\mathrm{cfg}}-1}) \\ H_{12}^2(\mathbf{q}_{N_{\mathrm{cfg}}}) \end{bmatrix} \quad (25)$$

where (see eq 16)

$$H_{12}^2(\mathbf{q}_K) = [H_{11}(\mathbf{q}_K) - \varepsilon_\Psi(\mathbf{q}_K)][H_{22}(\mathbf{q}_K) - \varepsilon_\Psi(\mathbf{q}_K)] \quad (26)$$

When first and second derivatives are available for H_{nn} and the ab initio energy, ε_Ψ, the derivative of the coupling terms can also be utilized in the DG fitting procedure. In this case, the $\mathbf{F}$ vector has the following elements

$$\mathbf{F} = \begin{bmatrix} H_{12}^2(\mathbf{q}_1) \\ \vdots \\ H_{12}^2(\mathbf{q}_{N_{\mathrm{cfg}}}) \\ \partial H_{12}^2(\mathbf{q}) \big/ \partial \mathbf{q}|_{\mathbf{q}=\mathbf{q}_1} \\ \vdots \\ \partial H_{12}^2(\mathbf{q}) \big/ \partial \mathbf{q}|_{\mathbf{q}=\mathbf{q}_{N_{\mathrm{cfg}}}} \\ \partial^2 H_{12}^2(\mathbf{q}) \big/ \partial \mathbf{q}^2|_{\mathbf{q}=\mathbf{q}_1} \\ \vdots \\ \partial^2 H_{12}^2(\mathbf{q}) \big/ \partial \mathbf{q}^2|_{\mathbf{q}=\mathbf{q}_{N_{\mathrm{cfg}}}} \end{bmatrix} \quad (27)$$

The corresponding unsymmetric matrix $\tilde{\mathbf{D}}$ contains the values and derivatives of the Gaussian bases

$$\tilde{\mathbf{D}} = \begin{bmatrix} g(\mathbf{q}_1, \mathbf{q}_1, \{i,j\}, \alpha_K) & \cdots & g(\mathbf{q}_1, \mathbf{q}_{N_{\mathrm{cfg}}}, \{i,j\}, \alpha_K) \\ \vdots & \ddots & \vdots \\ g(\mathbf{q}_{N_{\mathrm{cfg}}}, \mathbf{q}_1, \{i,j\}, \alpha_K) & \cdots & g(\mathbf{q}_{N_{\mathrm{cfg}}}, \mathbf{q}_{N_{\mathrm{cfg}}}, \{i,j\}, \alpha_K) \\ \partial g(\mathbf{q}, \mathbf{q}_1, \{i,j\}, \alpha_K) \big/ \partial \mathbf{q}|_{\mathbf{q}=\mathbf{q}_1} & \cdots & \partial g(\mathbf{q}, \mathbf{q}_{N_{\mathrm{cfg}}}, \{i,j\}, \alpha_K) \big/ \partial \mathbf{q}|_{\mathbf{q}=\mathbf{q}_1} \\ \vdots & \ddots & \vdots \\ \partial g(\mathbf{q}, \mathbf{q}_1, \{i,j\}, \alpha_K) \big/ \partial \mathbf{q}|_{\mathbf{q}=\mathbf{q}_{N_{\mathrm{cfg}}}} & \cdots & \partial g(\mathbf{q}, \mathbf{q}_{N_{\mathrm{cfg}}}, \{i,j\}, \alpha_K) \big/ \partial \mathbf{q}|_{\mathbf{q}=\mathbf{q}_{N_{\mathrm{cfg}}}} \\ \partial^2 g(\mathbf{q}, \mathbf{q}_1, \{i,j\}, \alpha_K) \big/ \partial \mathbf{q}^2|_{\mathbf{q}=\mathbf{q}_1} & \cdots & \partial^2 g(\mathbf{q}, \mathbf{q}_{N_{\mathrm{cfg}}}, \{i,j\}, \alpha_K) \big/ \partial \mathbf{q}^2|_{\mathbf{q}=\mathbf{q}_1} \\ \vdots & \ddots & \vdots \\ \partial^2 g(\mathbf{q}, \mathbf{q}_1, \{i,j\}, \alpha_K) \big/ \partial \mathbf{q}^2|_{\mathbf{q}=\mathbf{q}_{N_{\mathrm{cfg}}}} & \cdots & \partial^2 g(\mathbf{q}, \mathbf{q}_{N_{\mathrm{cfg}}}, \{i,j\}, \alpha_K) \big/ \partial \mathbf{q}^2|_{\mathbf{q}=\mathbf{q}_{N_{\mathrm{cfg}}}} \end{bmatrix} \quad (28)$$

where $\{i,j\}$ indicates that the columns of the matrix are elements obtained from cycling through all permutations denoted in the summation over these indices in eq 19. This square matrix has dimensions $DG_{\mathrm{dim}} = N_{\mathrm{cfg}} \times [1 + N_{\mathrm{dim}} + N_{\mathrm{dim}} \times (N_{\mathrm{dim}} + 1)/2]$. If the second derivatives of H_{12}^2 are unavailable, the dimensions of $\tilde{\mathbf{D}}$ are $N_{\mathrm{cfg}} \times (1 + N_{\mathrm{dim}})$. Additionally if the gradients are also unavailable, the matrix will have N_{cfg} rows. Once the solution to the $\mathbf{B}$ vector is known, eq 19 determines H_{12}^2 for all coordinates $\mathbf{q}$. The quality of the resulting PES, nonetheless, depends on the quality of the fit.

References

(1) Cook, M. J.; Katritzky, A. R.; Hepler, L. G.; Matsui, T. *Tetrahedron Lett.* **1976**, *31*, 2685.

(2) Beak, P. *Acc. Chem. Res.* **1977**, *10*, 186.

(3) Bensaude, O.; Dreyfus, M.; Dodin, G.; Dubois, J.-E. *J. Am. Chem. Soc.* **1977**, *99*, 4438.

(4) Guimon, C.; Garrabe, G.; Pfister-Guillouzo, G. *Tetrahedron Lett.* **1979**, *28*, 2585.

(5) Bensaude, O.; Chevrier, M.; Dubois, J.-E. *J. Am. Chem. Soc.* **1979**, *101*, 2423.

(6) Brown, R. S.; Tse, A.; Vederas, J. C. *J. Am. Chem. Soc.* **1980**, *102*, 1174.

(7) Scanlan, M. J.; Hillier, I. H.; MacDowell, A. A. *J. Am. Chem. Soc.* **1983**, *105*, 3568.

(8) Hatherley, L. D.; Brown, R. D.; Godfrey, P. D.; Pierlot, A. P.; Caminati, W.; Damiani, D.; Melandri, S.; Favero, L. B. *J. Phys. Chem.* **1993**, *97*, 46.

(9) Held, A.; Pratt, D. W. *J. Am. Chem. Soc.* **1993**, *115*, 9708.

(10) Maris, A.; Ottaviani, P.; Caminati, W. *Chem. Phys. Lett.* **2002**, *360*, 155.

(11) Frey, J. A.; Leist, R.; Tanner, C.; Frey, H.-M.; Leutwyler, S. *J. Chem. Phys.* **2006**, *125*, 114308.

(12) Hazra, M. K.; Samanta, A. K.; Chakraborty, T. *J. Chem. Phys.* **2006**, *125*, 214302.

(13) Hazra, M. K.; Chakraborty, T. *J. Phys. Chem. A* **2006**, *110*, 9130.

(14) Krebs, C.; Hofmann, H.-J.; Köhler, H.-J.; Weiss, C. *Chem. Phys. Lett.* **1980**, *69*, 537.

(15) Lledós, A.; Bertrán, J. *Tetrahedron Lett.* **1981**, *22*, 775.

(16) Schlegel, H. B.; Gund, P.; Fluder, E. M. *J. Am. Chem. Soc.* **1982**, *104*, 5347.

(17) Field, M. J.; Hillier, I. H. *J. Chem. Soc., Perkin Trans. II* **1987**, 617.

(18) Moreno, M.; Miller, W. H. *Chem. Phys. Lett.* **1990**, *171*, 475.

(19) Wong, M. W.; Wiberg, K. B.; Frisch, M. J. *J. Am. Chem. Soc.* **1992**, *114*, 1645.

(20) Del Bene, J. E. *J. Phys. Chem.* **1994**, *98*, 5902.

(21) Barone, V.; Adamo, C. *J. Phys. Chem.* **1995**, *99*, 15062.

(22) Wang, J.; Boyd, R. J. *J. Phys. Chem.* **1996**, *100*, 16141.

(23) Chou, P.-T.; Wei, C.-Y.; Hung, F.-T. *J. Phys. Chem. B* **1997**, *101*, 9119.

(24) Dkhissi, A.; Houben, L.; Smets, J.; Adamowicz, L.; Maes, G. *J. Mol. Struct.* **1999**, *484*, 215.

(25) Dkhissi, A.; Ramaekers, R.; Houben, L.; Adamowicz, L.; Maes, G. *Chem. Phys. Lett.* **2000**, *331*, 553.

(26) Alkorta, I.; Elguero, J. *J. Org. Chem.* **2002**, *67*, 1515.

(27) Müller, A.; Losada, M.; Leutwyler, S. *J. Phys. Chem. A* **2004**, *108*, 157.

(28) Piacenza, M.; Grimme, S. *J. Comput. Chem.* **2004**, *25*, 83.

(29) Li, Q.-S.; Fang, W.-H.; Yu, J.-G. *J. Phys. Chem. A* **2005**, *109*, 3983.

(30) Fu, A.; Li, H.; Du, D.; Zhou, Z. *J. Phys. Chem. A* **2005**, *109*, 1468.

(31) Tsuchida, N.; Yamabe, S. *J. Phys. Chem. A* **2005**, *109*, 1974.

(32) Esboui, M.; Jainane, N.; Lakhdar, Z. B. *Chem. Phys. Lett.* **2006**, *430*, 195.

(33) Wolfe, S.; Weinberg, N.; Hsieh, Y.-H. *Theor. Chem. Acc.* **2007**, *118*, 265.

(34) Hsieh, Y.-H.; Weinberg, N.; Wolfe, S. *Can. J. Chem.* **2008**, *86*, 81.

(35) Jensen, F. *Introduction to Computational Chemistry*, 2nd ed.; John Wiley & Sons Ltd.: West Sussex, England, 2007; pp 162−169.

(36) Grimme, S. *J. Chem. Phys.* **2003**, *118*, 9095.

(37) Venkatnathan, A.; Voth, G. A. *J. Chem. Theory Comput.* **2005**, *1*, 36.

(38) Ceotto, M.; Ayton, G. S.; Voth, G. A. *J. Chem. Theory Comput.* **2008**, *4*, 560.

(39) Schlegel, H. B.; Sonnenberg, J. L. *J. Chem. Theory Comput.* **2006**, *2*, 905.

(40) Sonnenberg, J. L.; Schlegel, H. B. *Mol. Phys.* **2007**, *105*, 2719.

(41) Curtiss, L. A.; Raghavachari, K.; Redfern, P. C.; Rassolov, V.; Pople, J. A. *J. Chem. Phys.* **1998**, *109*, 7764.

(42) Curtiss, L. A.; Redfern, P. C.; Raghavachari, K. *J. Chem. Phys.* **2007**, *126*, 84108.

(43) Montgomery, J. A.; Ochterski, J. W.; Petersson, G. A. *J. Chem. Phys.* **1994**, *101*, 5900.

(44) Martin, J. M. L.; de Oliveira, G. *J. Chem. Phys.* **1999**, *111*, 1843.

(45) Møller, C.; Plesset, M. S. *Phys. Rev.* **1934**, *46*, 618.

(46) Clark, T.; Chandrasekhar, J.; Spitznagel, G. W.; Schleyer, P. v. R. *J. Comput. Chem.* **1983**, *4*, 294.

(47) Krishnan, R.; Binkley, J. S.; Seeger, R.; Pople, J. A. *J. Chem. Phys.* **1980**, *72*, 650.

(48) Hratchian, H. P.; Schlegel, H. B. *J. Chem. Phys.* **2004**, *120*, 9918.

(49) Hratchian, H. P.; Schlegel, H. B. *J. Chem. Theory Comput.* **2005**, *1*, 61.

(50) Hratchian, H. P.; Schlegel, H. B. Finding minima, transition states, and follow reaction pathways on ab initio potential energy surfaces. In *Theory and Applications of Computational Chemistry: The First Forty Years*; Elsevier: New York, 2005; pp 195.

(51) Cancès, M. T.; Mennucci, B.; Tomasi, J. *J. Chem. Phys.* **1997**, *107*, 3032.

(52) Cossi, M.; Scalmani, G.; Rega, N.; Barone, V. *J. Chem. Phys.* **2002**, *117*, 43.

(53) Mennucci, B.; Cancès, M. T.; Tomasi, J. *J. Phys. Chem. B* **1997**, *101*, 10506.

(54) Frisch, M. J.; Trucks, G. W.; Schlegel, H. B.; Scuseria, G. E.; Robb, M. A.; Cheeseman, J. R.; Montgomery, J. A., Jr.; Vreven, T.; Scalmani, G.; Mennucci, B.; Barone, V.; Petersson, G. A.; Caricato, M.; Nakatsuji, H.; Hada, M.; Ehara, M.; Toyota, K.; Fukuda, R.; Hasegawa, J.; Ishida, M.; Nakajima, T.; Honda, Y.; Kitao, O.; Nakai, H.; Li, X.; Hratchian, H. P.; Peralta, J. E.; Izmaylov, A. F.; Kudin, K. N.; Heyd, J. J.; Brothers, E.; Staroverov, V.; Zheng, G.; Kobayashi, R.; Normand, J.; Sonnenberg, J. L.; Ogliaro, F.; Bearpark, M.; Parandekar, P. V.; Ferguson, G. A.; Mayhall, N. J.; Iyengar, S. S.; Tomasi, J.; Cossi, M.; Rega, N.; Burant, J. C.; Millam, J. M.; Klene, M.; Knox, J. E.; Cross, J. B.; Bakken, V.; Adamo, C.; Jaramillo, J.; Gomperts, R.; Stratmann, R. E.; Yazyev, O.; Austin, A. J.; Cammi, R.; Pomelli, C.; Ochterski, J. W.; Ayala, P. Y.; Morokuma, K.; Voth, G. A.; Salvador, P.; Dannenberg, J. J.; Zakrzewski, V. G.; Dapprich, S.; Daniels, A. D.; Strain, M. C.; Farkas, O.; Malick, D. K.; Rabuck, A. D.; Raghavachari, K.; Foresman, J. B.; Ortiz, J. V.; Cui, Q.; Baboul, A. G.; Clifford, S.; Cioslowski, J.; Stefanov, B. B.; Liu, G.; Liashenko, A.; Piskorz, P.; Komaromi, I.; Martin, R. L.; Fox, D. J.; Keith, T.; Al-Laham, M. A.; Peng, C. Y.; Nanayakkara, A.; Challacombe, M.; Chen, W.; Wong, M. W.; Pople, J. A. *Gaussian DV*; revision G.01; Gaussian, Inc.: Wallingford, CT, 2007.

(55) *Mathematica*; 5.2 ed.; Wolfram Research: Champaign, IL, 2005.

(56) Sonnenberg, J. L.; Schlegel, H. B. The Empirical Valence Bond Toolkit for Mathematica. http://chem.wayne.edu/schlegel/ (accessed November, 2008).

(57) Case, D. A.; Darden, T. A.; Cheatham, T. E., III.; Simmerling, C. L.; Wang, J.; Duke, R. E.; Luo, R.; Crowley, M.; Walker, R. C.; Zhang, W.; Merz, K. M.; Wang, B.; Hayik, S.; Roitberg, A.; Seabra, G.; Kolossvary, I.; Wong, K. F.; Paesani, F.; Vanicek, J.; Wu, X.; Brozell, S. R.; Steinbrecher, T.; Gohlke, H.; Yang, L.; Tan, C.; Mongan, J.; Hornak, V.; Cui, G.; Mathews, D. H.; Seetin, M. G.; Sagui, C.; Babin, V.; Kollman, P. A. *AMBER 10*; University of California: San Francisco, 2008.

(58) Takahashi, K.; Kramer, Z. C.; Vaida, V.; Skodje, R. T. *Phys. Chem. Chem. Phys.* **2007**, *9*, 3864.

(59) Villa, J.; Warshel, A. *J. Phys. Chem. B* **2001**, *105*, 7887.

(60) Balint-Kurti, G. G. *Adv. Chem. Phys.* **1975**, *30*, 137.

(61) London, F. *Z. Elektrochem.* **1929**, *35*, 552.

(62) Eyring, H. *Trans. Farad. Soc.* **1938**, *34*, 3.

(63) Evans, M. G.; Polanyi, M. *Trans. Farad. Soc.* **1938**, *34*, 11.

(64) Ogg, R. A.; Polanyi, M. *Trans. Farad. Soc.* **1934**, *31*, 604.

(65) Evans, M. G.; Warhurst, E. *Trans. Farad. Soc.* **1938**, *34*, 614.

(66) Warshel, A.; Weiss, R. M. *J. Am. Chem. Soc.* **1980**, *102*, 6218.

(67) Pross, A.; Shaik, S. S. *J. Am. Chem. Soc.* **1982**, *104*, 187.

(68) Chang, Y.-T.; Miller, W. H. *J. Phys. Chem.* **1990**, *94*, 5884.

(69) Chang, Y.-T.; Minichino, C.; Miller, W. H. *J. Chem. Phys.* **1992**, *96*, 4341.

(70) Minichino, C.; Voth, G. A. *J. Phys. Chem. B.* **1997**, *101*, 4544.

(71) Higashi, M.; Truhlar, D. G. *J. Chem. Theory Comput.* **2008**, *4*, 790.

(72) Albu, T. V.; Corchado, J. C.; Truhlar, D. G. *J. Phys. Chem. A* **2001**, *105*, 8465.

(73) Kim, Y.; Cochado, J. C.; Villa, J.; Xing, J.; Truhlar, D. G. *J. Chem. Phys.* **2000**, *112*, 2718.

(74) Lin, H.; Pu, J.; Albu, T. V.; Truhlar, D. G. *J. Phys. Chem. A* **2004**, *108*, 4112.

(75) Saad, Y.; Schultz, M. H. *SIAM J. Sci. Stat. Comput* **1986**, *7*, 856.

(76) Pulay, P. *Chem. Phys. Lett.* **1980**, *73*, 393.

(77) Pulay, P. *J. Comput. Chem.* **1982**, *3*, 556.

(78) Pulay, P. Direct inversion in interative subspace (DIIS). In *Molecular Quantum Mechanics: Analytic Gradients and Beyond*; Csaszar, A. G., Fogarasi, G., Schaefer, H. F., III., Szalay, P. G., Eds.; ELTE Institute of Chemistry: Budapest, Hungary, 2007; pp 71.

(79) Shaik, S. S.; Schlegel, H. B.; Wolfe, S. *Theoretical Aspects of Physical Organic Chemistry: The SN2 Mechanism*; John Wiley & Sons, Inc.: New York, 1992.

(80) Rappé, A. K.; Casewit, C. J.; Colwell, K. S.; Goddard, W. A., III.; Skiff, W. M. *J. Am. Chem. Soc.* **1992**, *114*, 10024.

CT800477Y